Surface-plasmon spectrum of Ag(001) measured by high-resolution angle-resolved electron-energy-loss spectroscopy

M. Rocca, F. Biggio, and U. Valbusa
Centro di Fisica delle Superfici e Basse Temperature del Consiglio Nazionale delle Ricerche, Dipartimento di Fisica, via Dodecaneso 33, I-16146 Genova, Italy
(Received 4 April 1990)

An angle-resolved high-resolution electron-energy-loss-spectroscopy study is reported of the surface-plasmon spectrum on Ag(001) along different azimuths. A single loss energy is observed which disperses linearly with exchanged momentum $q_{\parallel}$ from 3.69 ± 0.01 eV with a slope of 1.5 ± 0.1 eV Å. The data were recorded for different impact energies and scattering angles. Within experimental accuracy, no dependence of plasmon frequency and dispersion on the crystal azimuth was observed. The peak width measures 95 meV at small wave vectors and broadens linearly with $q_{\parallel}$. Beyond 0.10 $Å^{-1}$ the width increases drastically because of the opening of efficient damping channels connected with interband transitions involving the *d* bands. Plasmon energy on Ag(100) agrees with the value reported for Ag(111) by Suto *et al.* and by Contini and Layet, while the form of the dispersion curves differs remarkably, being linear instead of quadratic as in the case of (111) and (110) surfaces.

INTRODUCTION

In spite of the importance of the surface-electronic excitation spectrum, little is known about surface-plasmon energies and dispersion at metallic surfaces. Plasmon-energy losses were studied for thin films by use of high-energy electron scattering long ago, showing that surface structures can be extremely sharp, as in the case of silver[1,2] or simple metals.[3] Angle-resolved high-resolution low-energy electron-energy-loss spectroscopy (EELS) was applied only recently to this field: surface-plasmon dispersion on silver was studied by Contini and Layet[4] for Ag(111) and by Suto *et al.*[5] for Ag(111) and Ag(110); simple-metal films were investigated by Tsuei *et al.*[6] While for simple-metal surfaces a linear dispersion was observed for small plasmon wave vector $q_{\parallel}$, in accord with the predictions of the jellium model,[6] on silver single crystals the dispersion was found to be quadratic[4,5] and the plasmon energy was found to depend on the crystal face and, for Ag(110), also on azimuthal orientation.[5] These results show the complexity of surface-plasmon spectra of noble-metal surfaces and emphasize the need for a widened experimental basis.

In this paper we report on an EELS study of Ag(001) performed along both the high-symmetry directions ⟨100⟩ and ⟨110⟩ and off ⟨100⟩ [see Fig. 1(a) for the surface unit cell]. We find at vanishing $q_{\parallel}$ a plasmon energy of 3.69 eV and a dispersion independent of crystal direction. The dispersion behaves linearly in $q_{\parallel}$. In addition, a study of plasmon width has been performed. The plasmon loss was found to be a very narrow structure near $q_{\parallel}=0$, which broadens linearly with $q_{\parallel}$ initially slowly and then rapidly beyond 0.10 $Å^{-1}$.

The paper is organized as follows: First, we describe the experimental setup; then the experimental results are presented. In the following two sections a broad discussion of plasmon dispersion and damping is given.

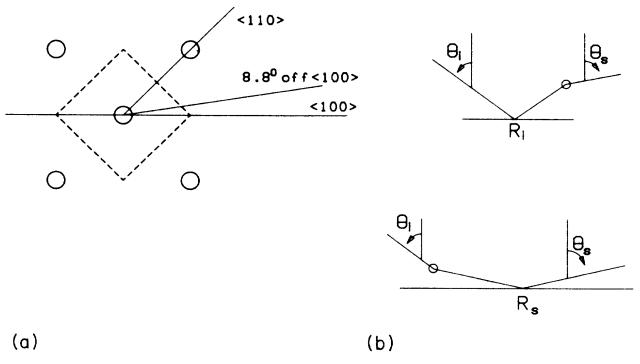

FIG. 1. (a) Surface structure of Ag(100). The indicated directions are those in which the experiment was performed. (b) Scattering geometry: reflection before loss and loss before reflection amplitudes add up to the inelastic intensity. θ_i and θ_s are incident and scattering angles. Reflection factors R_i and R_s may differ both in amplitude and in phase.

EXPERIMENT

The experiment was performed in ultrahigh vacuum (low-10^{-10}-mbar range) with a new apparatus which is described elsewhere.[7] Here we will report only those details which are of importance for plasmon-dispersion measurements. The sample is a silver single crystal whose surface is aligned within 0.25° with the (001) plane. Crystal temperature can be varied between 120 and 1000 K and is measured by Chromel-Alumel thermocouple. The surface was cleaned in vacuum by cycles of Ne^{+} sputtering followed by annealing at 700 K. Care was taken not to heat the sample above this temperature to avoid

crystal evaporation and reconstruction. The quality of the surface was checked by low-energy electron diffraction (LEED) and Auger-electron spectroscopy (AES). At the end of the cleaning procedure no peak due to vibrational modes of adsorbed species was detected by EELS. The azimuthal orientation of the crystal was checked by LEED and could be set within 2° from the desired direction. The EEL spectra were recorded with our single-pass CDA 127° spectrometer, whose impact energy can be selected between 1 and 300 eV. Scattering and incidence angles, θ_s and θ_i, can be positioned between 40° and 90° with respect to the normal [see Fig. 2(b)], with the constraint that $\theta_s - \theta_i \geq 80°$. In the experiment the energy resolution ΔE_i of the primary beam was lowered to 20 meV in order to improve the signal-to-noise ratio for off-specular measurements.

Momentum and energy conservation of the electrons determine momentum transfer $q_\parallel$ for each choice of incident angle θ_i, scattering angle θ_s, incident energy E_i, and energy loss E_{loss} according to the kinematical relation

$$q_\parallel = \sqrt{2mE_i}/\hbar(\sin\theta_i - \sqrt{1-E_{\text{loss}}/E_i}\sin\theta_s) \ . \quad (1)$$

The dispersion curves were measured by fixing E_i and θ_s and positioning θ_i according to Eq. (1) as illustrated in Fig. 1. The resolution in momentum space, $\Delta q_\parallel$, can be obtained from Eq. 1 and reads

$$\Delta q_\parallel \simeq \sqrt{2mE_i}/\hbar(\cos\theta_i + \sqrt{1-E_{\text{loss}}/E_i}\cos\theta_s)\Delta\theta_s \ . \quad (2)$$

Equation (2) does not take into account the error on E_i since in the present experiment this contribution is negligible. When the angular aperture of the dipole lobe, $\beta = E_{\text{loss}}/2E_i$, is larger than $\Delta\theta_s$ (i.e., for $E_i > 120$ eV), $\Delta\theta_s$ is the angular acceptance α of the EEL spectrometer. α can be determined by measuring the full width at half maximum (FWHM) of the angular distribution of the specular peak. Since $\alpha = (\Delta\theta_i^2 + \Delta\theta_s^2)^{1/2}$, $\Delta\theta_i \simeq \Delta\theta_s$, and $\alpha = 1.5°$, it follows that $\Delta\theta_i = \Delta\theta_s \simeq 1°$. As one can see from Eq. (2), $\Delta q_\parallel$ is lowest at low impact energy and grazing incidence. Most of the measurements presented in this paper were recorded in this limit. For higher impact energies, $\beta < \Delta\theta_s$, so that the dipole lobe is inside the specular beam. In this case $\theta_i = \theta_s$ and Eq. (1) reduces to

$$q_\parallel = (\sqrt{2mE_i}/\hbar)\beta\sin\theta_s \ , \quad (3)$$

and, consequently, $\Delta q_\parallel$ reduces to

$$\Delta q_\parallel = (\sqrt{2mE_i}/\hbar)2\cos\theta_s\,\Delta\theta_s \ , \quad (4)$$

where $\Delta\theta_s$ is now the width of the dipole lobe β.

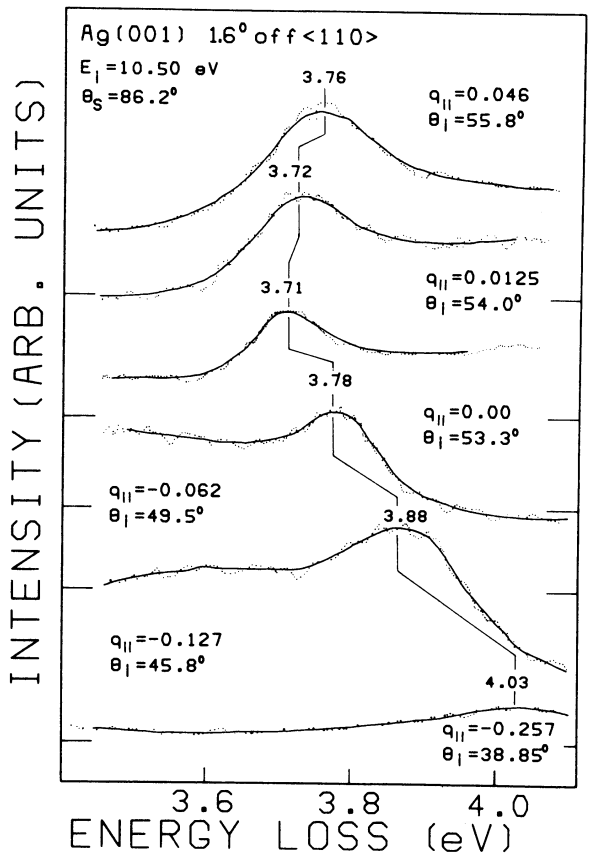

FIG. 2. Set of measurements for $E_i = 10.5$ eV, $\theta_s = 86.2°$, and different θ_i; 1.6° off ⟨100⟩. The $q_\parallel$ value is calculated according to Eq. (1) for the plasmon loss and is given in Å^{-1}.

RESULTS

Three sets of data are shown in Figs. 2–4 that correspond to runs performed at grazing incidence and at different impact energies. The azimuthal orientation in the measurements, as determined by LEED, reads 1.6° off ⟨100⟩ (Fig. 2), 8.8° off ⟨100⟩ (Fig. 3), and 2° off ⟨110⟩ (Fig. 4). Other data were recorded for E_i ranging between 10 and 120 eV and θ_s between 42° and 87° for the same azimuthal directions. In all cases a single well-defined energy-loss feature was observed. The spectra were recorded at room temperature.

The raw data were digitalized and smoothed according to the following equation:

$$Y(n) = \{4y(n) + 2[y(n-1) + y(n+1)] + [y(n-2) + y(n+2)]\}/10 \ , \quad (5)$$

where y is the intensity of the scattered electrons in the nth channel. Linear regression on m points was then applied on the smoothed set of data Y to find the slope on each point that was integrated to yield the solid curve. The maximum of the peak was eventually determined by a parabolic fit on m points. The choice of m depends on the quality of the spectrum, and was typically 25.

As one can see from Figs. 2–4, plasmon energy shifts

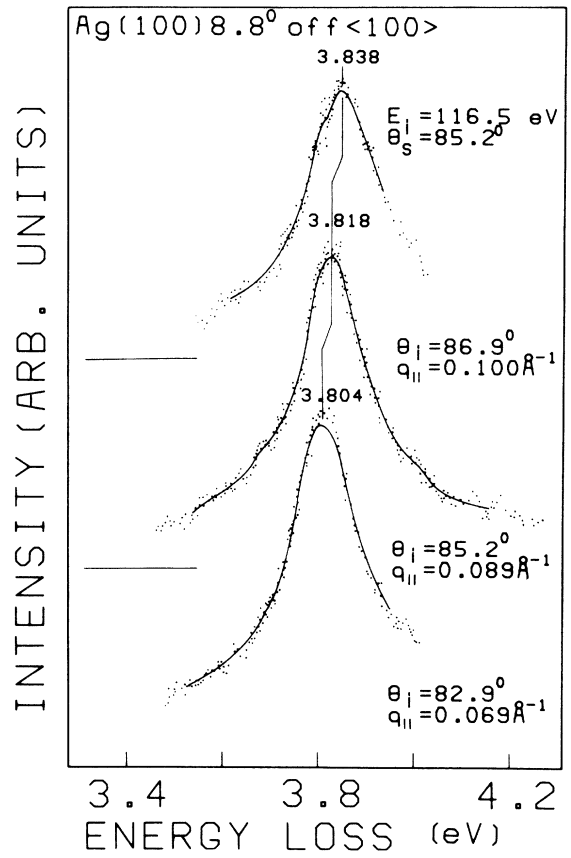

FIG. 3. Same as Fig. 1, but for $E_i = 116.5$ eV and $\theta_s = 85.2°$; 8.8° off ⟨100⟩.

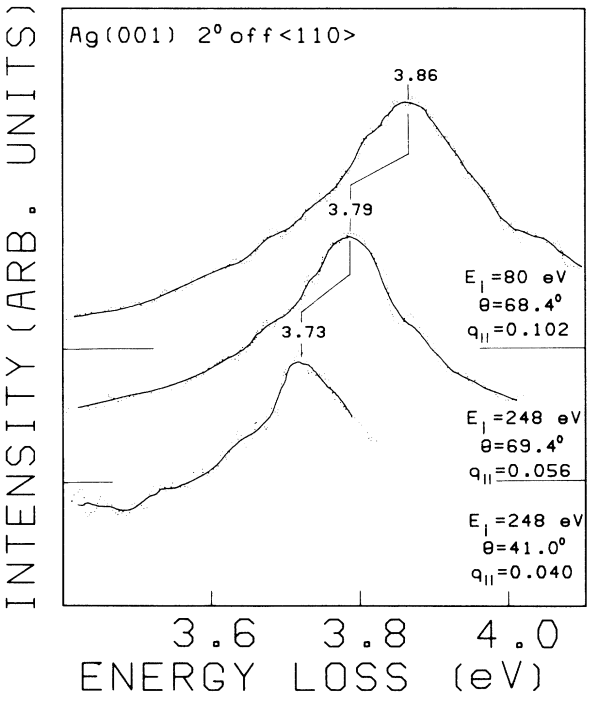

FIG. 4. Collection of measurements taken in specular for different θ_s and E_i; 2° off ⟨110⟩; $q_\parallel$ is measured in Å^{-1}.

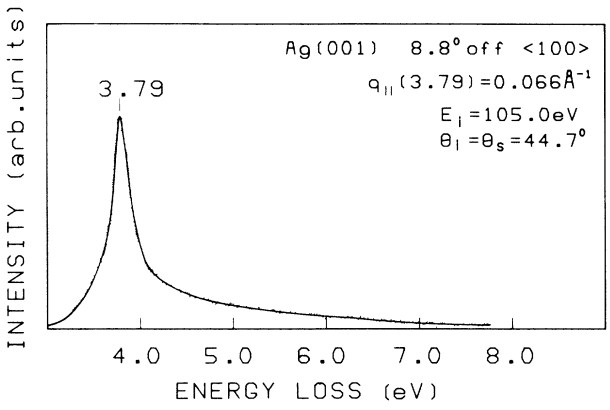

FIG. 5. Energy-loss spectrum for $E_i = 105$ eV and $\theta_s = 44.7°$. No losses are present apart from the plasmon.

linearly upwards with exchanged momentum, while peak width broadens initially slowly and then more rapidly. Data taken at high impact energy display only the plasmon loss, as demonstrated in Fig. 5. In most spectra the plasmon loss is evidently asymmetric because of the presence of a high-energy tail, as in Fig. 5. The tail could be associated with the onset of interband transitions or to multipole plasmons, as recently suggested for simple metals.[8] Under particular experimental conditions, this tail can be enhanced by rapid changes in inelastic cross section,[9] as in Fig. 2.

The spectra reported in Fig. 2 show the plasmon peak superimposed on a structured background, a feature common to most measurements recorded at low E_i. We suggest that this contribution is of dipolar origin and is associated to electron-hole–pair excitations. Its intensity is proportional to the elastic reflectivity R [see Fig. 1(b)], which oscillates with impact energy; in addition, near Rydberg resonances, R_i or R_s can vary abruptly over orders of magnitude[10] and can mimic energy-loss peaks. An example of such structures is given in Fig. 6 by the

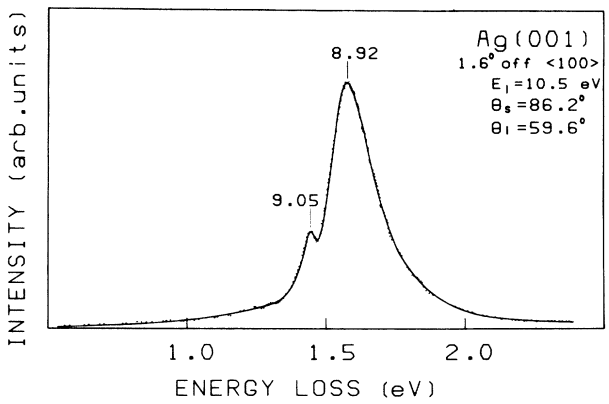

FIG. 6. Energy-loss spectrum taken off specular showing false energy-loss features. They arise from rapid variations of the elastic reflection coefficient near Rydberg resonance conditions. These features are, in fact, connected to reflectivity variations at $E_i - E_{\text{loss}} = 9.05$ and 8.92 eV.

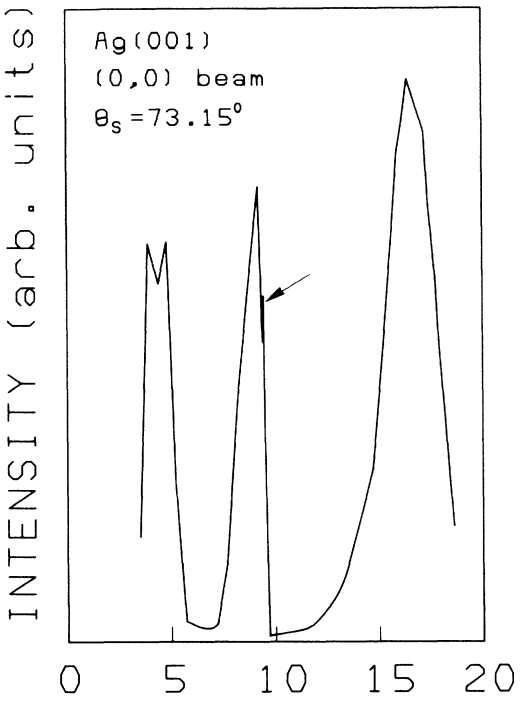

FIG. 7. Intensity vs impact energy for the (00) beam. The extremely sharp intensity variations at 9.45 eV are due to Rydberg resonances.

apparent energy losses at 1.45 and 1.58 eV. These losses, corresponding to absolute electron energies of 9.05 and 8.92 eV, are only related to a variation of elastic reflectivity, as demonstrated in Fig. 7, where the sharp intensity changes near 9.45 eV are due to Rydberg resonances. The difference in energy between the structures in Figs. 6 and 7 is caused by different scattering geometries. Similar features were already observed on Ni(110),[11] and can be recognized by the fact that the apparent loss energy depends on impinging energy. The relation between R and E_i becomes smoother at higher impact energies, but in this case $\Delta q_\parallel$ becomes prohibitively large for plasmon-dispersion measurements.

DETERMINATION OF PLASMON DISPERSION AND ENERGY

All measured plasmon energies are reported plotted against exchanged momentum in Fig. 8 separated according to azimuthal orientation along (a) ⟨100⟩, (b) off ⟨100⟩, and (c) ⟨110⟩. The $q_\parallel$ corresponding to the measured frequency was determined according to Eq. (1). The error bars indicate $\Delta q_\parallel$ calculated by Eq. (2) or (4), depending on E_i. In order to avoid systematic errors in angle determination, we carried out, where possible, measurements at both positive and negative $q_\parallel$. The $q_\parallel = 0$ position was then determined experimentally by analyzing symmetry properties of the plasmon-dispersion curve with respect to it. The maximum departure from the expected zero value was 0.007 Å^{-1}, as reported in a previous paper.[9] In addition, loss-peak position can also be shifted by strong variations in inelastic-scattering cross section, as also demonstrated in Ref. 9. The spread of data points beyond $q_\parallel = 0.15$ Å^{-1} is caused by reflectivity changes inside the width of the peaks which influence the determination of the position of the maximum.

The sets of data have been fitted with

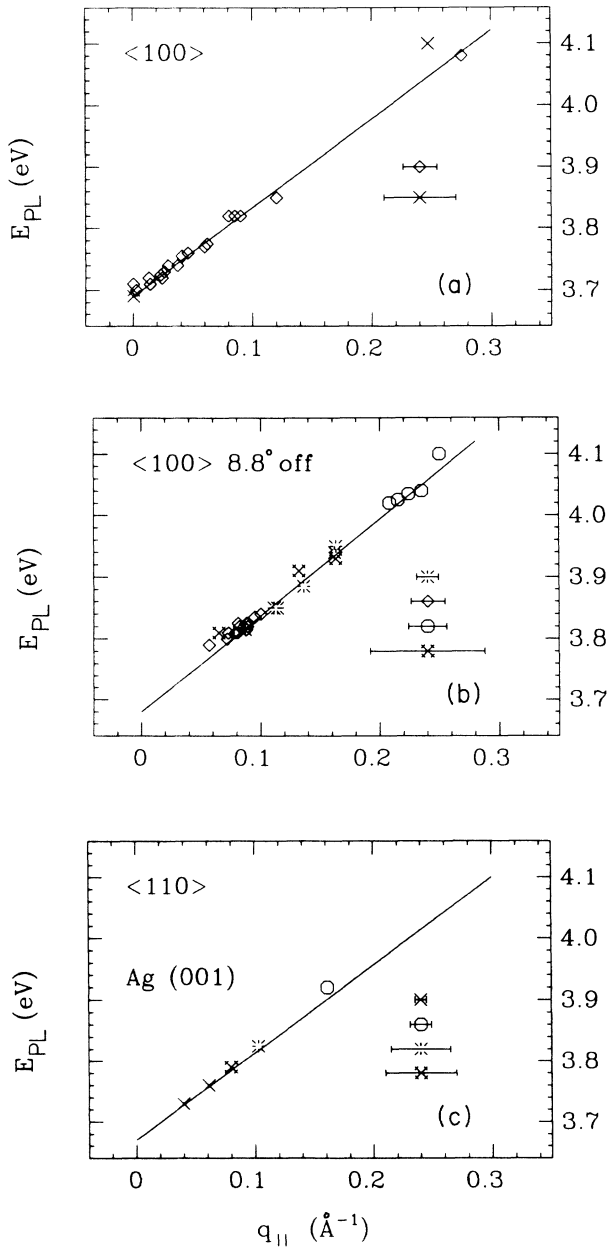

FIG. 8. Collection of plasmon energies vs exchanged momentum. (a) ⟨100⟩: ◇—$E_i = 10.5$–17 eV, $\theta_s = 75°$–90°; ×—$E_i = 10.5$–17 eV, $\theta_s = 45°$–60°. (b) 8.8° off ⟨100⟩: ⋇—$E_i = 38.5$ or 76 eV, $\theta_s = 75°$–85°; ◇—$E_i = 116$–127 eV, $\theta_s = 80°$–85°; ○—$E_i = 20$ eV, $\theta_s = 75°$–85°; ⤫—$E_i = 24$ eV, $\theta_s = 45°$–60°. (c) ⟨110⟩: ×—$E_i = 248$ eV, $\theta_s = 41.6°$; ×—$E_i = 217$ eV, $\theta_s = 69.4°$; ○—$E_i = 36$ eV, $\theta_s = 73.2°$; ⋇—$E_i = 80$ eV, $\theta_s = 68.4°$; ⤫—$E_i = 130$ eV, $\theta_s = 69.4°$. The result of the best fit to the data is given by the solid lines. The parameters are taken from Table I.

TABLE I. Values of parameters a and b of Eq. (6) obtained by fitting the experimental dispersion curves along the ⟨100⟩ and ⟨110⟩ directions. Best fit is performed by χ^2 minimization. [The lines obtained with the best-fit values reported in this table are shown in Figs. 8(a) (⟨100⟩), 8(b) (8.8° off ⟨100⟩), 8(c) (⟨110⟩), and 9 (⟨100⟩ and 8.8° off ⟨100⟩).]

Direction	a (eV)	b (eV Å)	χ^2
⟨100⟩	3.69±0.01	1.4±0.1	4.0×10^{-2}
8.8° off ⟨100⟩	3.68±0.02	1.6±0.1	4.3×10^{-2}
⟨110⟩	3.67±0.01	1.6±0.1	2.9×10^{-2}
⟨100⟩ and 8.8° off ⟨100⟩	3.69±0.01	1.5±0.1	6.7×10^{-2}

$$E_{\rm pl}=a+bq_{\parallel} \tag{6}$$

and

$$E_{\rm pl}=a+bq_{\parallel}+cq_{\parallel}^2 , \tag{7}$$

taking into account the different errors on the experimental points. The best-fit–parameter values and uncertainties have been computed by minimizing the χ^2 values by using the MINUIT computing routine. These parameters, together with the χ^2 values, are reported in Tables I and II. As one can see, the quadratic contribution is negligible and the linear coefficient is compatible for all directions studied. In Fig. 9, data taken along ⟨100⟩ and 8.8° off ⟨100⟩ are reported. Data along ⟨110⟩ are systematically lower in energy by 20 meV with respect to ⟨100⟩, although this discrepancy is at the limit of present experimental accuracy. Similar azimuthal dependence was observed by Petri *et al.*[12] for bulk plasmons of Al and attributed to electron-correlation effects.

The plasmon energy on Ag(001) coincides at vanishing $q_{\parallel}$ with the value reported for Ag(111).[4,5] The disagreement with high-energy inelastic-scattering data (3.63 eV for silver foils[1]) can probably be explained by a small amount of roughness present in films, which can cause a shift of the plasmon to lower frequencies.[13] Moreover, we find a steep linear dispersion in contrast to the quadratic behavior reported for (111) (Refs. 4 and 5) and (110) (Ref. 5) surfaces. The present data coincide for large $q_{\parallel}$ with the dispersion reported by Zacharias and Kliever[14] for thin silver films, which was attributed to the bulk plasmon. A comparison between (111), (100), and (110) surfaces is presented in Fig. 10. The crystal-face dependence of plasmon energy and dispersion is not surprising for a noble metal such as Ag because the electronic spectrum in the bulk and at the surface differs from face to face,[15] and interband transitions therefore contribute differently to the surface dielectric response. We have no physical explanation for the quadratic and linear behavior of plasmon dispersion on the different crystallographic faces of silver. A face anisotropy in surface-plasmon dispersion has also been reported for Al by inelastic low-energy electron diffraction (ILEED) measurements by Duke *et al.*[16] The experimental uncertainty of ILEED is, however, too large to allow one to draw reliable conclusions.

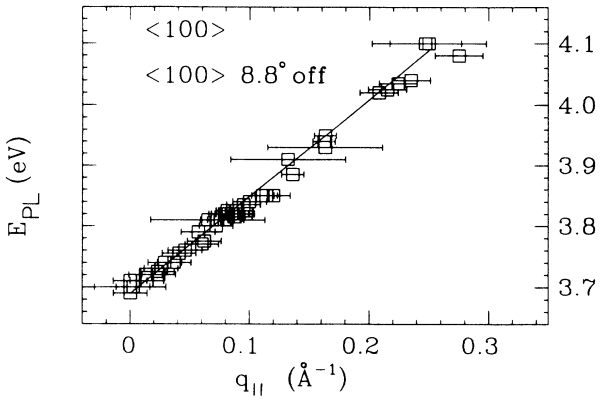

FIG. 9. Collection of plasmon energies vs $q_{\parallel}$ for data taken along ⟨100⟩ and 8.8° off ⟨100⟩. The solid line indicates the best fit with the parameters of Eq. (6) as reported in Table I.

According to the jellium model, the dispersion relation of the surface plasmon at small wave vector should be linear in $q_{\parallel}$ and have a slope proportional to the position of the centroid of the induced charge $d(\omega)$ with respect to the edge of jellium:[17,18]

$$E_{\rm SP}(q_{\parallel})=E_{\rm SP}(0)[1-\tfrac{1}{2}d(\omega_s)q_{\parallel}+o(q_{\parallel}^2)] , \tag{8}$$

where $E_{\rm SP}(0)$ is the surface-plasmon frequency at $q_{\parallel}=0$. $d(\omega_s)$ being a positive quantity the Bohm-Pines random-phase-approximation (RPA) formulation, leads to a negative plasmon dispersion. The jellium model is, however, not applicable to noble metals. We can therefore only speculate that the positive slope is indicative of an excess of electrons at the surface. Such an excess would indicate a relaxation of the outer interlayer spacing. A small relaxation is not in conflict with the measured phonon spectrum.[5,19]

TABLE II. Values of parameters a, b, and c of Eq. (7) obtained by fitting the experimental dispersion curves along ⟨100⟩ and ⟨110⟩ directions. Best fit is performed by χ^2 minimization.

Direction	a (eV)	b (eV Å)	c (eV Å^2)	χ^2
⟨100⟩	3.69±0.01	1.4±0.1	0.06±0.44	4.6×10^{-2}
8.8° off ⟨100⟩	3.73±0.02	0.8±0.2	2.8±0.9	4.3×10^{-2}
⟨110⟩	3.68±0.01	1.3±0.2	1.3±1.0	1.0×10^{-2}
⟨100⟩ and 8.8° off ⟨100⟩	3.69±0.01	1.4±0.1	0.5±0.6	6.4×10^{-2}

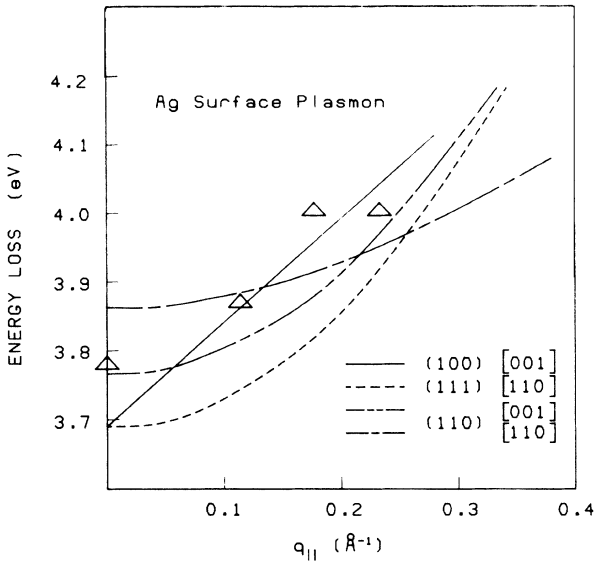

FIG. 10. Comparison between our results for Ag(001) and those of Suto *et al.* for Ag(111) and Ag(011) (Ref. 5). The triangles indicate volume plasmon losses according to Zacharias and Kliever (Ref. 14).

PLASMON DAMPING

The FWHM of the energy-loss peaks, ΔE_{loss}, is depicted in Fig. 11 plotted against $q_{\|}$. The error bar refers to $\Delta q_{\|}$ calculated using Eq. (2) or (4). The FWHM grows slowly for small $q_{\|}$ and increases drastically beyond a critical value $q_{\|c} \simeq 0.10$ Å^{-1} with a linear behavior in $q_{\|}$ both below and above $q_{\|c}$. No difference was noticed between the explored crystallographic directions; the data are therefore reported all together. Fitting the points below and above $q_{\|c}$ separately, with

$$\Delta E_{\text{loss}} = A + Bq_{\|} , \tag{9}$$

one obtains $A = 0.092 \pm 0.005$ eV and $B = 1.00 \pm 0.10$ eV Å ($\chi^2 = 0.43$) below 0.10 Å^{-1}, and $A = -0.26 \pm 0.05$ eV and $B = 4.4 \pm 0.3$ eV Å ($\chi^2 = 0.29$) above 0.10 Å^{-1}. The crossing between the two lines occurs at $q_{\|c} = 0.10 \pm 0.02$ Å^{-1}. The corresponding critical value in energy, E_{plc}, can be calculated from $q_{\|c}$ values using the linear relation found for plasmon dispersion and reads 3.84 ± 0.03 eV. E_{plc} determines the threshold of the opening of efficient damping channels connected to interband transitions. According to theoretical calculations of Eckhardt *et al.*,[20] for bulk silver the onset of strong transitions involving the *d* bands should lie at 3.72 eV instead of 3.84 eV, as we find.

The quadratic dependence of the surface-plasmon linewidth was observed by Tsuei *et al.* for potassium films, and was also reported for bulk plasmons.[21,22] The present surface is therefore the first system on which a linear dependence of ΔE_{loss} versus $q_{\|}$ has been observed. It is interesting to note that jellium theory, although not suited for noble metals, predicts a linear dependence of ΔE_{loss} versus $q_{\|}$ because of damping associated with

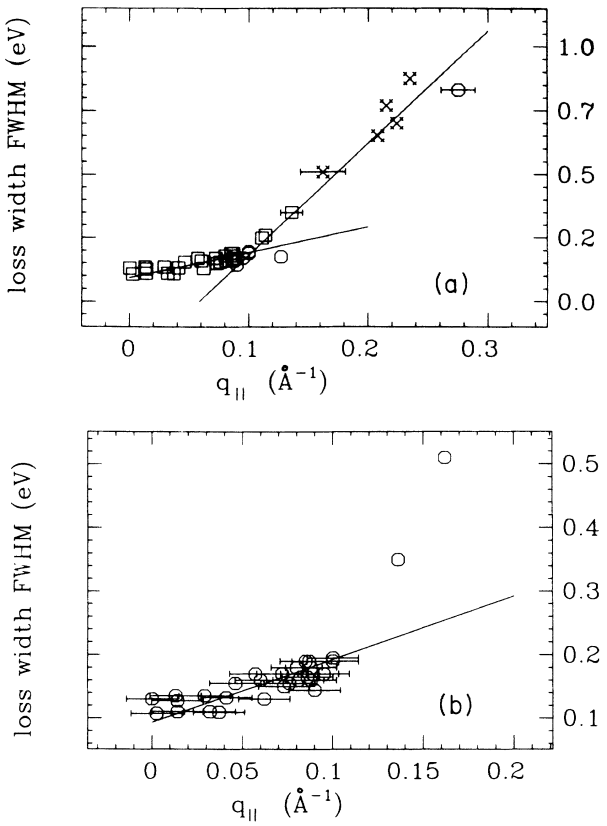

FIG. 11. (a) Collection of plasmon widths vs momentum. (b) Same as (a) for the data below 0.1 Å^{-1}. The lines are best-fit curves, as discussed in the text.

electron-hole–pair excitations.[23] Theory predicts, however, a vanishing width at $q_{\|} = 0$, in contrast to the present experiment.

At vanishing $q_{\|}$ the plasmon loss is extremely narrow. The value of ΔE_{pl}, the width of the plasmon loss, can be extracted by deconvoluting the experimental data of Fig. 11. The experimental width ΔE_{loss} is, in fact, given by

$$\Delta E_{\text{loss}} = (\Delta E_{\text{pl}}^2 + \Delta E_{\text{expt}}^2)^{1/2} , \tag{10}$$

where ΔE_{expt} is the experimental resolution, which can be determined, by use of Eq. (6), from $\Delta q_{\|}$ and the experimental uncertainty of the impact energy ΔE_i. As an example, for $E_i = 16$ eV, $\theta_s = 81.6°$, and $\theta_i = 60°$, one obtains $\Delta E_{\text{expt}} = 52$ meV, which is due to the $\Delta q_{\|}$ uncertainty for 48 meV and to ΔE_i for 20 meV. In this case, since $\Delta E_{\text{loss}} = 110$ meV, $\Delta E_{\text{pl}} = 95$ meV. This value is comparable with that reported for bulk plasmons on silver,[2] 75 meV.

CONCLUSIONS

In conclusion, we have performed measurements of surface-plasmon dispersion for Ag(100) along different

crystallographic directions. The data differ remarkably from those reported for thin films[1] and for the other low-Miller-index surfaces of silver.[3,4] In particular, we find a linear dispersion, in contrast to the quadratic one reported for (111) and (110) surfaces. A linear dependence was also found for plasmon damping, at least below 0.10 Å^{-1}.

ACKNOWLEDGMENTS

We thank B. Gumhalter, B. Persson, and A. Liebsch for fruitful discussions, and K. D. Tsuei for having sent us a copy of Ref. 5 prior to publication. The technical assistance of G. Maloberti, A. Gussoni, and P. Pozzo is greatly appreciated.

[1] J. Daniels, Z. Phys. **203**, 235 (1967).
[2] P. Zacharias, Z. Phys. **238**, 172 (1970).
[3] K. J. Krane and H. Raether, Phys. Rev. Lett. **37**, 1355 (1976).
[4] R. Contini and J. M. Layet, Solid State Commun. **64**, 1179 (1987).
[5] S. Suto, K. D. Tsuei, E. W. Plummer, and E. Burstein, Phys. Rev. Lett. **63**, 2590 (1989).
[6] K. D. Tsuei, E. W. Plummer, and P. J. Feibelman, Phys. Rev. Lett. **63**, 2256 (1989).
[7] A. Gussoni, G. Maloberti, L. Racca, M. Rocca, and U. Valbusa (unpublished).
[8] K. D. Tsuei, E. W. Plummer, A. Liebsch, K. Kempa, and P. Bakshi, Phys. Rev. Lett. **64**, 44 (1990).
[9] M. Rocca and U. Valbusa, Phys. Rev. Lett. **64**, 2398 (1990).
[10] R. O. Jones and P. J. Jennings, Surf. Sci. Rep. **9**, 165 (1988).
[11] D. Rebenstorff, H. Ibach, and J. Kirschner, Solid State Commun. **56**, 885 (1985).
[12] E. Petri, A. Otto, and W. Hanke, Solid State Commun. **19**, 711 (1976).
[13] T. S. Rahman and A. A. Maradudin, Phys. Rev. B **21**, 2137 (1980).
[14] P. Zacharias and K. L. Kliever, Solid State Commun. **18**, 23 (1976).
[15] N. Altmann, V. Dose, and A. Goldmann, Z. Phys. B **65**, 171 (1986).
[16] C. B. Duke, L. Pietronero, J. O. Porteus, and J. F. Wendelken, Phys. Rev. B **12**, 4059 (1975).
[17] P. J. Feibelman, Prog. Surf. Sci. **12**, 287 (1982).
[18] A. Liebsch, Phys. Sci. **35**, 354 (1987).
[19] M. Rocca, L. Risso, B. Vicenzi, and U. Valbusa, Surf. Sci. **216**, 153 (1989); P. Moretto, M. Rocca, U. Valbusa, and J. Black, Phys. Rev. B **41**, 12 905 (1990).
[20] H. Eckhardt, L. Fritsche, and J. Noffke, J. Phys. F **14**, 97 (1984).
[21] T. Kloos, Z. Phys. **265**, 225 (1973).
[22] H. Raether, in *Excitation of Plasmons and Interband Transitions by Electrons,* Vol. 88 of *Springer Tracts in Modern Physics,* edited by G. Höhler (Springer, Berlin, 1980), p. 65.
[23] P. J. Feibelman, Phys. Rev. B **9**, 5077 (1974).